A Sensor for Trace H_2O Detection in D_2O

Samuel G. Dunning[1, 5], Ana J. Nuñez[1, 2, 5], Matthew D. Moore[1, 5], Alexander Steiner[3], Vincent M. Lynch[1], Jonathan L. Sessler[1], Bradley J. Holliday[4], Simon M. Humphrey[1, 6, *]

email: smh@cm.utexas.edu

[1]Department of Chemistry, University of Texas at Austin, 6.336 Norman Hackerman Building, 100 East 24th Street, Stop A1590, Austin, TX 78712, USA

[2]Dow Chemical Company, Midland, MI 48667, USA

[3]Department of Chemistry, University of Liverpool, Crown Street, Liverpool L69 7ZD, UK

[4]Austin, TX, USA

*Corresponding author

[5]Co-first author

[6]Lead Contact

Summary

PCM-22, a metal-organic framework material comprising triphenylphosphine and Ln^{3+} ions (Ln = Pr–Yb), exhibits solid-state luminescence at room temperature. Mixed-metal versions of PCM-22 that contain controlled amounts of Eu^{3+}, Gd^{3+}, and Tb^{3+} function as highly sensitive, broad-scope solid-state sensors that can rapidly identify unknown solvents by providing a unique "eight-factor" fingerprint. The sensors allow for immediate solvent identification via color changes that are obvious to the naked eye and also permit quantitative chemical analysis by uncomplicated spectrophotometry. These same materials achieve quantitative detection of H_2O in D_2O from 10 to 120,000 ppm. The detection of trace H_2O is also demonstrated in a range of common solvents, including those incompatible with conventional laboratory titration methods.

A series of luminescent phosphine coordination materials show diverse sensing capabilities. These solid-state sensor materials can detect trace H_2O impurities in D_2O from 10 to 120,000 ppm and can rapidly identify unknown solvents.

Introduction

The photoluminescent properties of lanthanide (Ln)-based materials play an important role in modern light-emitting devices,[1] optoelectronics,[2] and chemical sensors.[3] The emission characteristics of Ln^{3+} ions are particularly attractive for sensor development because their emission bands are narrow, occur predominantly in the visible and near-infrared spectral regions, and are highly element specific and their emission wavelengths are generally not perturbed by their coordination environments. Ln^{3+} ions are not easy to directly excite by incident photoradiation; therefore, indirect excitation is more commonly employed. Typically, this is achieved by incorporation of Ln^{3+} ions into organic chromophores.[4] Light harvesting by the chromophore and efficient internal energy transfer to the Ln^{3+} ions results in Ln-based emission, often with high photoluminescent quantum yields (Φ_{PL}).[5] Light emission from excited Ln ions is quenched by vibrational coupling to certain chemical bonds (e.g., O–H, N–H, and C–H). The emissive Φ_{PL} values of Ln-based complexes are therefore often acutely diminished in solution and in the presence of ambient moisture, thus limiting their applicability in devices. However, because the relative degree of quenching is directly related to the concentration and identity of the chemical bond(s) causing the quenching, Ln ions can be exploited as quantitative probes for a variety of analytes.[6–8] A recognized challenge is to produce a stable, robust, sensitive, and tunable solid-state material that would allow these features to be exploited for sensing. Here, we report one such approach based on an organophosphine-based metal-organic framework (MOF). This system permits broad solvent identification and can detect and quantify trace amounts of H_2O in D_2O, as well as in a range of organic solvents. To the best of our knowledge, no previously reported examples of any material-based sensors are capable of detecting trace amounts of H_2O in D_2O—a highly challenging type of detection.

MOFs have emerged as ideal candidates for the preparation of new solid-state chemical sensors. MOFs are microporous crystalline materials with well-defined periodic structures and high surface areas.[9] MOFs prepared with Ln^{3+}ions as the integral structural components provide access to materials with a high volumetric density of structurally identical emission centers, which enables a large photoluminescent sensor response from a small quantity of material.[10]Rational design principles in MOF chemistry also permit a degree of control over Ln–Ln separation distances in the solid state. Such tunability allows for optimization of the luminescence properties; this parameter is virtually impossible to control in the solution phase. To date, a number of Ln-MOFs with specific sensing capabilities have been reported, for example, in the selective detection of anions,[11] explosives,[12] pH,[13] temperature,[14] and toxic contaminants.[15] Despite this, Ln-MOFs have not yet been shown to have the ability to act as universally applicable sensors because of chemical incompatibility with a broad range of analytes and their inability to achieve the required limits of detection.

We have developed a unique family of MOFs based on arylphosphine ligands, referred to as phosphine coordination materials (PCMs). PCMs have a high volumetric density of guest-accessible Lewis basic P(III) sites inside the pores, which present a range of possibilities for solid-state chemical modifications. Unlike the types of ligands commonly utilized in MOF synthesis (i.e., planar poly(carboxylated) aromatics), trigonal pyramidal R_3P ligands constitute 3D building blocks that provide access to rare network topologies.[16,17]In previous work, we demonstrated that tris(*p*-carboxylato)triphenylphosphine ($P(C_6H_4$-*p*-$CO_2H)_3$; $tctpH_3$) is an effective chromophore that allows for the efficient excitation of a number of Ln^{3+} ions.[18] A recently identified material, named PCM-22, was prepared by direct reaction of $Ln(NO_3)_3$ and ($tctpH_3$) in an aqueous-organic-solvent mixture at 80°C. PCM-22 can be prepared

in good yields with any Ln^{3+} source from Pr–Yb. Isostructural materials can also be prepared with mixtures of two or more Ln^{3+} ions, resulting in systems in which the ions are incorporated randomly throughout the lattice.

We show here that mixed-Ln versions of PCM-22 with systematically varied molar amounts of Eu^{3+} (a visible red-light emitter), Tb^{3+} (a visible green-light emitter), and Gd^{3+} (non-emissive in the visible region) can be used for rapidly differentiating between a wide range of solvents through a characteristic "eight-factor" fingerprint. These materials can also be used for visually indicating and spectrophotometrically quantifying the presence of trace water on the ppm scale in multiple solvents, including acetone, ethanol, and acetonitrile, which are incompatible with conventional water-detection methods (e.g., the standard Karl-Fisher titration[19]). Most notably, quantitative detection over the 10–120,000 ppm H_2O range in D_2O was achieved. D_2O is virtually physically indistinguishable from regular water; in addition to its use as a neutron moderator in nuclear reactors,[20] high-purity D_2O is important in a myriad of spectroscopic and synthetic applications.[21] Simple and quantitative analysis of D_2O purity is desirable, yet detection by atomic absorption spectroscopy[22] or nuclear magnetic resonance can only detect down to 1%–5%.[23] Infrared laser spectroscopy can achieve ppm-level detection[24,25] but is not convenient for rapid point-of-need detection.

Results and Discussion

Synthesis, Structure, and Solid-State Luminescence of Ln-PCM-22 Materials

Deprotonated $tctp^{3-}$ phosphine was reacted with $Ln(NO_3)_3$ to give charge-neutral and highly symmetric polymers with the formula unit $[Ln(tctp)(OH_2)_3]\cdot 3$(1,4-dioxane). As seen from the single-crystal X-ray diffraction structure of the Tb^{3+} version, PCM-22 consists of puckered 2D honeycomb sheets that are stacked in an eclipsed arrangement to give an infinite 3D solid with large hexagonal channels (Figure 1). Each Ln^{3+} center has nine coordinating ligands comprising three facial bis(chelating) carboxylates and three OH_2 ligands (Figure 1A). Alternating 3-connected phosphine-*P* and Ln^{3+} nodes give rise to infinite puckered sheets of fused hexagonal rings (Figures 1B and 1C). The 3,3-connected lattice topology is the same as that exhibited by the metallic phases of the group 15 elements (Figure 1D).[26] PCM-22 inhabits the rarely observed polar space group $P3c1$; opposite faces of each sheet are chemically distinct (composed of either Ln or P atoms), and individual sheets are inherently chiral (adjacent sheets consist of the other enantiomer).

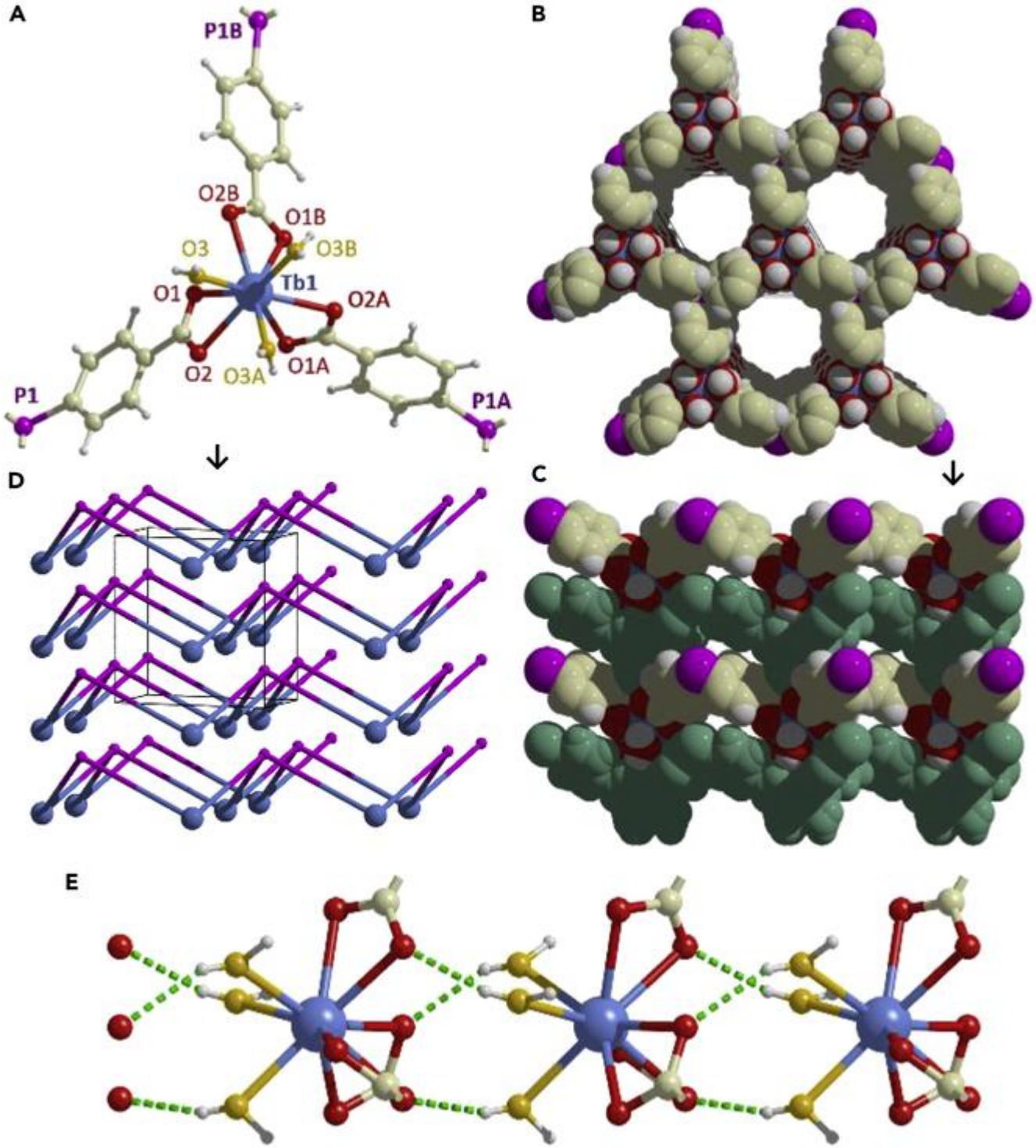

Figure 1 Chemical Structure of PCM-22(A) Nodal connectivity in Tb-PCM-22.(B) Space-filling view along the c axis shows 1D hexagonal channels.(C) Space-filling view perpendicular to the channel direction shows close stacking of adjacent sheets (alternate sheets are shown in green for clarity).(D) 3,3-connected net version of (C) (P, pink; Tb, blue).(E) The closest inter-layer O···H interactions (dashed green bonds).

The eclipsed close stacking of sheets in PCM-22 (Figures 1C and 1D) is similar to that observed in covalent organic frameworks, where inter-layer π-π interactions dominate the supramolecular organization.[27] Such stacking of 2D sheets to give ordered pseudo-3D materials results in large pores. Eclipsed packing is unusual for 2D MOFs, which more commonly adopt staggered-layer conformations that result in smaller void spaces,[28] as previously observed for

Zn^{2+}-based PCMs constructed with the same ligand.[29] In PCM-22, eclipsing of sheets is ascribed to a network of close-range inter-layer hydrogen-bonding interactions between the Ln-bound OH_2 ligands and the carboxylate-*O* atoms (Figure 1E). The shortest O···O distances are 2.74 Å. Adjacent sheets are densely packed, resulting in Ln···Ln inter-layer distances of 5.77 Å (Figure 1C). The hexagonal channels have a maximum van der Waals accessible opening of 14.5 Å.

All forms of Ln-PCM-22 from Pr–Yb were synthesized according to the same procedure. Powder X-ray diffraction (PXRD) analysis confirmed the products as being isostructural (see Figure S1). Thermogravimetric analysis (TGA) provided support for the conclusion that the solvent of crystallization (1,4-dioxane; see Figure S2) present in the channels of the as-synthesized materials could be completely removed by heating to 100°C (observed, 29.5; calculated, 30.4 wt %). A further distinct mass loss was observed between 100°C and 190°C, which was attributed to the loss of a single coordinated H_2O molecule per Ln^{3+}center (observed, 3.6; calculated, 3.1 wt %). This observation was supported by quantitative D_2O emissive lifetime studies (see below). Above 190°C, no further mass loss occurred until the onset of framework decomposition at ca. 450°C. For all sensing studies, bulk samples were desolvated under vacuum at 75°C–100°C for 18 hr, resulting in BET (Brunauer, Emmett, and Teller) surface areas of between 303 and 455 $m^2\ g^{-1}$ (CO_2, 196 K; see Figure S3).

The accepted antenna mechanism[30] responsible for Ln-centered emission in MOFs occurs by the generation of ligand-centered triplet (T_1) excited states, followed by ligand-to-metal energy transfer. Energy transfer is most efficient when the T_1 level of the organic chromophore is ca. 2,000–4,000 cm^{-1} above the excited state of the Ln^{3+} ion.[30,31] The phosphorescence spectrum of free tctpH_3dissolved in a frozen glass of 2-methyltetrahydrofuran at 77 K gave T_1 = 24,390 cm^{-1}. When incorporated into PCM-22, the T_1 state of the $tctp^{3-}$ ligand shifted slightly (T_1 = 25,253 cm^{-1} at 77 K; obtained from the [non-emissive] Gd-PCM-22 surrogate; see Figure S4). On the basis of the excited-state energies of Tb^{3+} ($^5D_4$ = 20,366 cm^{-1}),[30,31] we chose Tb-PCM-22 to assess the fundamental luminescence properties as a function of solvation.

The room-temperature emission spectrum of an as-synthesized sample of Tb-PCM-22 displayed features characteristic of Tb^{3+} emission with well-resolved electronic transitions between 491 and 648 nm, ascribed to $^7F_J \leftarrow {}^5D_4$ relaxations (J = 6, 5, 4, 3, 2; see Figure S5). In comparison with previous, Tb^{3+}-based MOFs (Φ_{PL} = 22%–90%[32]), the average value observed for Tb-PCM-22 (Φ_{PL} = 57% ± 3%) was somewhat surprising because each Tb^{3+} is coordinated by three H_2O molecules, and the structure also contains closely interacting 1,4-dioxane solvent molecules, both of which are known emission quenchers (see Figures 1E and S6). However, it is also known that the quenching efficacy of coordinated solvent decreases when hydrogen-bonding interactions perturb the normal vibrational frequencies of the oscillators that are responsible for quenching (e.g., O–H bonds in the case of H_2O).[33]

The number of H_2O molecules present within the quenching sphere of an emissive Ln^{3+} ion (q) can be approximated by comparison of the emissive lifetime with an analogous material prepared with OD_2 ligands. For Tb-PCM-22, this yielded q = 3.4 ± 0.5 OH_2 per Tb^{3+}, in agreement with all other characterization data. When the same Tb-PCM-22 sample was desolvated in vacuo at 75°C, the solid-state luminescence was dramatically diminished (Φ_{PL} = 10.6%). The corresponding temperature-dependent PXRD analysis indicated a loss of bulk crystallinity (see Figure S7); temperature-dependent Fourier transform infrared spectroscopy likewise showed a decrease in the intensity of the stretching bands, attributed to coordinated OH_2 above 80°C (ca. 3,400 cm^{-1}; see Figure S8); in addition, exposure of the desolvated sample to a D_2O-saturated N_2 atmosphere resulted in an emissive lifetime change corresponding to the

loss of one OH_2 ligand per Tb^{3+} (see Figure S9). Collectively, these observations are in direct agreement with the TGA studies (see above).

Luminescence quenching as a consequence of desolvation has been observed previously in the solid state.[34] The loss of site symmetry of individual Ln^{3+} ions coupled to a decrease in the inter-layer Tb···Tb distances upon desolvation is likely to enable more non-radiative relaxation pathways. Through-space metal-to-metal energy transfer is only consequential between ions separated by <10 Å.[35] The intra-layer Ln···Ln separation distance in PCM-22 is 13.7 Å, and significant contraction is not possible within each 2D sheet. In comparison, the inter-layer Tb···Tb separation distance when solvated is only 5.77 Å. Desolvation and removal of one OH_2 ligand from each Ln^{3+} disrupts the well-ordered H-bonding network, inducing disorder between adjacent 2D sheets and resulting in a loss of bulk crystallinity. In support of the idea that inter-layer Ln···Ln energy transfer is modulated by solvation, when the poorly emissive desolvated materials were re-exposed to the mother liquor (1:1:1 *N*,*N*-dimethylformamide [DMF]/dioxane/H_2O), the luminescence intensity was recovered in a matter of seconds (Figure 2; Φ_{PL} = 65% after 5s, 91% after 300 s). In addition, PXRD analysis confirmed that the initial bulk diffraction features were restored (see Figures S10 and S11). PCM-22 appears to display a soft crystalline behavior,[36] whereby solid-state structural reorganization is possible without permanent loss of long-range order.

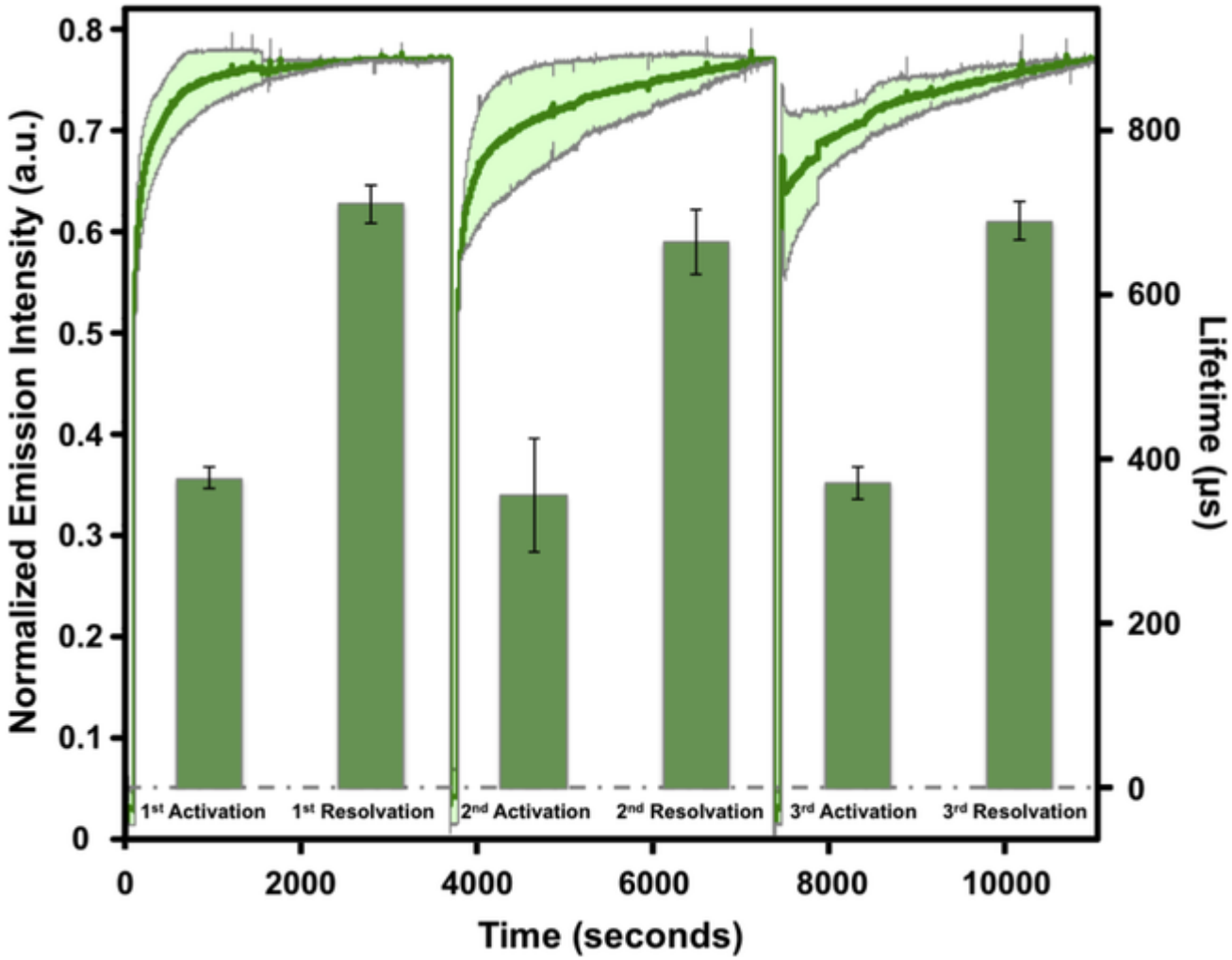

Figure 2 On-Off Luminescence of Tb-PCM-22Temporal luminescence intensity response for Tb-PCM-22 upon three consecutive cycles of desolvation-resolvation; the light-green region shows the measurement error obtained from three independent studies. Inset: bar graphs showing the measured emissive lifetimes upon cycling.

The on-off luminescence switching behavior was preserved upon further cycles of desolvation and exposure to fresh solvent, without any marked loss of emission intensity or response time (Figure 2). The measured emissive lifetimes (Figure 2, inset) confirmed that the recovery of Tb^{3+}-centered emission was independent of changing surface characteristics of the crystallites upon desolvation and resolvation.[31] Finally, to rule out the alternative possibility, namely that the observed emission recovery upon resolvation was due to physical dissolution and recrystallization, we immersed a sample of desolvated Tb-PCM-22 in solvent and continually monitored it over a period of 15 days under an optical microscope equipped with a charge-coupled device camera. The macroscopic shape and volume of the crystals remained unchanged during this time, and there was no evidence of nucleation of new crystallites (see Figure S12).

Trace H_2O Detection in D_2O and Other Solvents by Eu:Tb-PCM-22

The incorporation of multiple lanthanides in MOFs can provide access to desirable hybrid emission properties.[37] PCM-22 is particularly amenable toward incorporation of multiple Ln^{3+} ions in the standard synthetic protocol. Moreover, comparable product yields were obtained. We prepared a series of mixed Eu:Tb-PCM-22 materials to further probe the nature of inter-layer Ln···Ln energy transfer. Eu^{3+} is emissive in the red visible spectral region but has an excited-state energy that is significantly lower than that of $tctp^{3-}$. As a result, less effective sensitization was seen than for Tb^{3+} ($^7F_2 \leftarrow\!\!- {}^5D_0$ = 17,250 cm^{-1}; Eu-PCM-22 Φ_{PL} = 11% ± 4%). On the other hand, Eu^{3+} is known to undergo efficient excitation via downhill energy transfer from the $^5D_4$ Tb^{3+} excited state.[38] Thus, a notable change in emission color is predicted upon desolvation of Eu:Tb-PCM-22 with a commensurate decrease in inter-layer Ln···Ln separation.

The observed emission color of as-synthesized Eu_x:Tb_y-PCM-22 was found to be continually tunable as a direct function of the relative site occupancies (x, y) of the randomly distributed Eu^{3+} and Tb^{3+} ions (Figure 3A). The emission profile of the as-synthesized Eu_1:Tb_1-PCM-22 showed net yellow emission. The normalized intensities of peaks at 616 and 543 nm (Tb^{3+} and Eu^{3+}, respectively) gave a ratio of I_{543nm} / I_{616nm} = 0.78. Upon desolvation in vacuo, the emission color became distinctly red with I_{543nm} / I_{616nm} = 0.54 (see Figure S13). This finding is evidence of $Tb^{3+} \rightarrow Eu^{3+}$ energy down-transfer that becomes favored as the Tb^{3+}···Eu^{3+} contact distances decrease upon desolvation. It is also consistent with the Förster resonance energy-transfer mechanism.[31] The Eu^{3+} emissive lifetimes measured for a range of Eu:Tb systems also showed a positive correlation with the Tb^{3+} concentration (τ_{Eu3+} = 243–624 μs for 0%–90% Tb^{3+}, respectively; see Table S1).

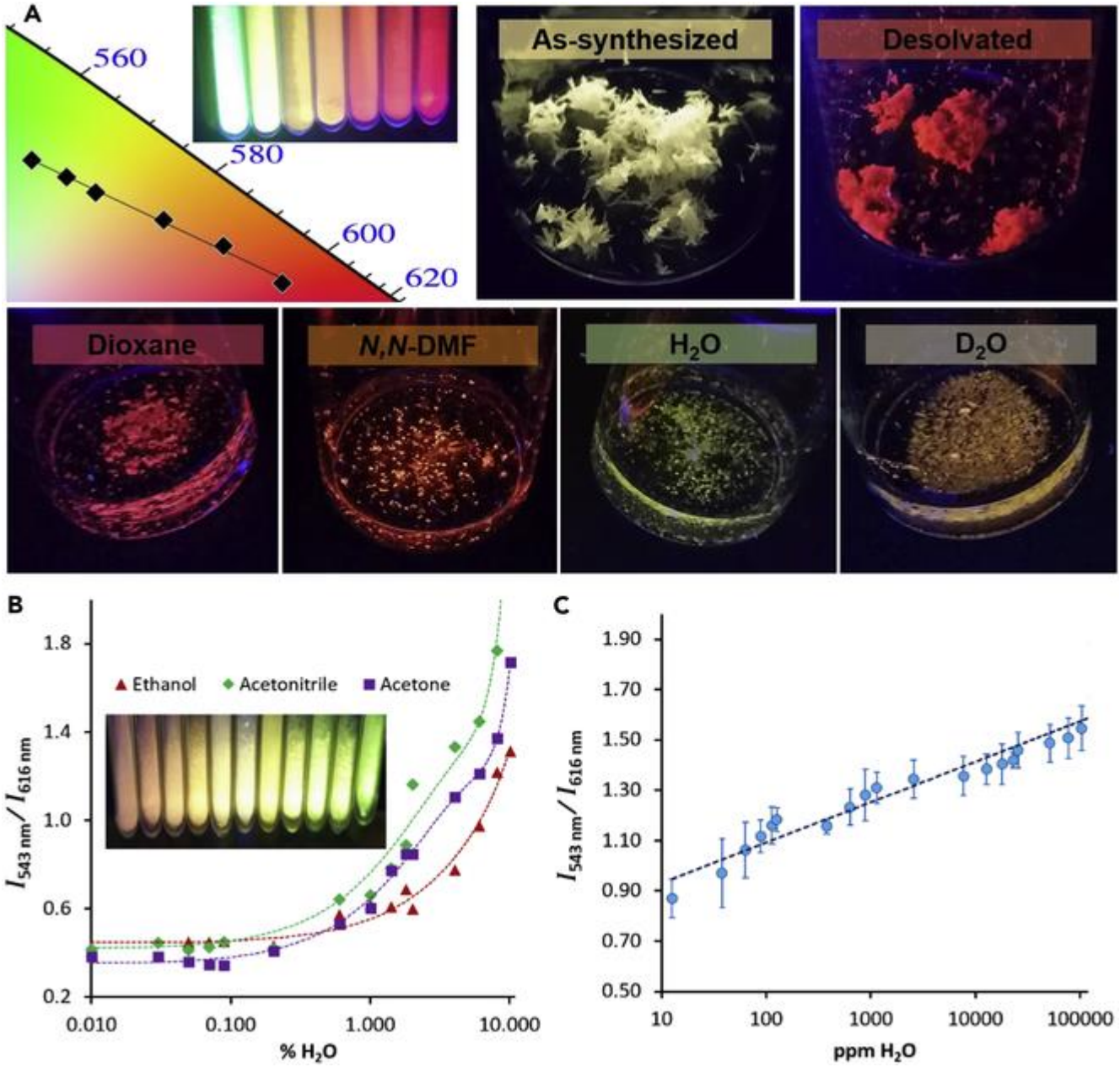

Figure 3 Trace H_2O Sensing Using Eu_X:Tb_Y-PCM-22(A) Top left: CIE chart for various Eu:Tb-PCM-22 compositions and their corresponding CIE coordinates upon excitation at 365 nm; inset: photograph of the materials (Eu:Tb = 1:0, 5:1 3:1, 1:1, 1:3, 1:5, 0:1). Top right: photos of as-synthesized and desolvated Eu_1:Tb_1-PCM-22. Bottom: upon exposure of the same desolvated material to four different solvents (dioxane, DMF, H_2O, and D_2O).(B) Relative photoemission response ratio curves upon addition of H_2O to activated Eu_1:Tb_5-PCM-22 samples that had been pre-soaked in dry solvents (ethanol, acetonitrile, and acetone). Inset: the visual response upon addition of H_2O to acetone.(C) Relative photoemission response ratios obtained upon addition of trace H_2O to Eu_1:Tb_5-PCM-22 pre-soaked in D_2O show a linear response. Error bars were obtained from three separate experiments.

Re-exposure of the Eu:Tb materials to the DMF/dioxane/H_2O mother liquor resulted in recovery of the original mixed-site emission, accompanied by restoration of bulk crystallinity. However, to our surprise, when desolvated samples of Eu:Tb-PCM-22 were resolvated with the individual components of the mother liquor, a unique emission profile and readily

visualized color was obtained for each solvent: red for DMF, orange for dioxane, and green for H_2O (Figure 3A). Whereas most other organic solvents induced smaller differences in emission intensities than the activated samples, materials exposed to H_2O displayed large emission changes ($I_{543nm} / I_{616nm} = 1.61$), ascribed to enhanced quenching of the Eu^{3+} excited state by H_2O.

To explore Eu:Tb-PCM-22 as a possible trace water detector, we optimized the metal ratio to give the greatest red-to-green color contrast in response to addition of trace quantities of H_2O (Eu_1:Tb_5; see Figure S14). The limits of detection were then assessed for trace H_2O in acetone, acetonitrile, ethanol, and D_2O for the reasons described above. The mixed Eu_1:Tb_5-PCM-22 could quantify H_2O down to 0.1% v/v in these organic solvents; it also provided a visual response to H_2O between 0.5% and 5% (Figure 3B, inset). This sensor material also had the remarkable ability to detect H_2O in D_2O in the range of 10–100 ppm (Figure 3C). Organic solvents showed a non-linear relationship between H_2O concentration and the corresponding I_{543nm} / I_{616nm} ratio, presumably because H_2O is able to coordinate directly to vacant Ln^{3+} sites. In contrast, the sensor response for H_2O in D_2O was essentially linear over the entire range of 10–120,000 ppm. Presumably, this reflects the fact that sites within the material were already fully solvated by coordinated OD_2 before trace amounts of H_2O were introduced. Because the O–D oscillator is a less effective Ln^{3+} excited-state quencher than O–H (particularly for Eu^{3+}), the observed change in the I_{543nm} / I_{616nm} ratio is ascribed to OH_2/OD_2 exchange.

Ternary Eu:Gd:Tb-PCM-22 Materials for Eight-Factor Solvent Fingerprinting

To improve the sensitivity of PCM-22 toward a much broader range of analytes, a series of three-metal sensor materials (Eu_1:Gd_1:Tb_1, Eu_3:Gd_1:Tb_1, Eu_1:Gd_3:Tb_1, and Eu_1:Gd_1:Tb_3) were synthesized (for exact molar ratios, see Table S2). Gd^{3+} was employed as a site dilutant; it is non-emissive in the visible region because of a large separation between the $^6P_{7/2}$ excited state and $^8S_{7/2}$ground states, which inhibits ligand-to-metal energy transfer.[31] Gd^{3+}-based emission was not observed in the materials (ca. 315 nm). Instead, the ternary sensors displayed a broad emission band (ca. 510 nm) ascribed to ligand-based phosphorescence, which was not prominent in the binary metal sensors. The introduction of Gd^{3+} ions reduced the proportion of close-range $Tb^{3+}\cdots Eu^{3+}$interactions.

The Eu:Gd:Tb-PCM-22 materials were desolvated and exposed to 18 common solvents with diverse chemical functionalities and polarities (with dielectric constants, ε_r = 1.89–79.8). The resulting emission spectra were recorded for the generation of a unique eight-factor fingerprint profile for each solvent (Figure 4). The eight factors are derived from the emission CIE coordinates for the four Eu:Gd:Tb compositions and the relative emission intensities of each ($I_{relative} = \{(I_{543nm} / I_{616nm}) / I_{510nm}\}$; see Figure S15). For the 18 solvents tested, the eight-factor fingerprints obtained were spectroscopically unique: Eu:Gd:Tb-PCM-22 acts as a sensor for very rapid solvent identification, which is internally calibrated by the monitoring of relative intensities at three wavelengths with only one excitation wavelength.

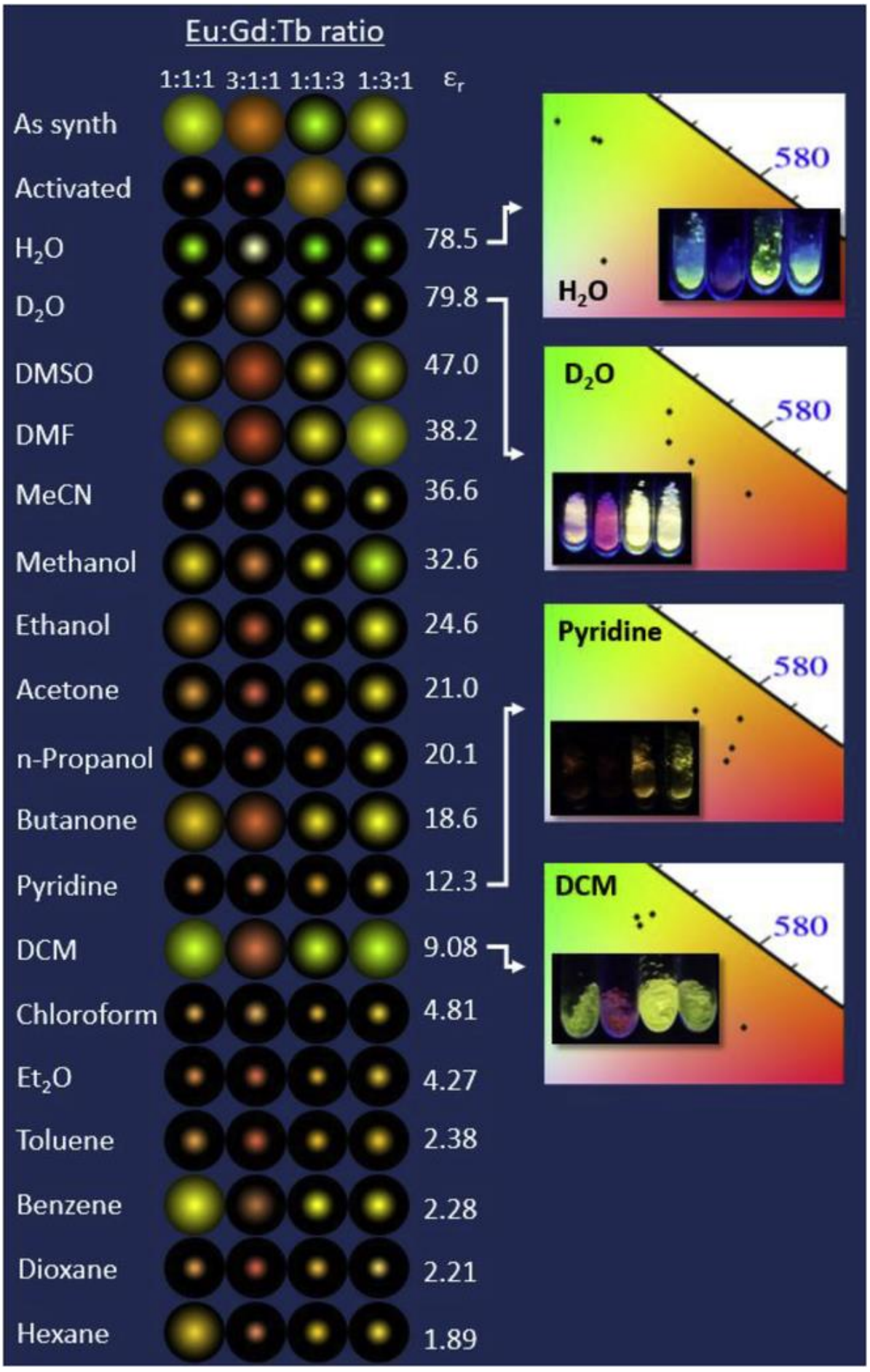
Eu:Gd:Tb ratio
1:1:1 3:1:1 1:1:3 1:3:1 ε_r
As synth
Activated
H_2O 78.5
D_2O 79.8
DMSO 47.0
DMF 38.2
MeCN 36.6
Methanol 32.6
Ethanol 24.6
Acetone 21.0
n-Propanol 20.1
Butanone 18.6
Pyridine 12.3
DCM 9.08
Chloroform 4.81
Et_2O 4.27
Toluene 2.38
Benzene 2.28
Dioxane 2.21
Hexane 1.89
580
H_2O
D_2O
Pyridine
DCM

Figure 4 Broad Solvent Sensing Using Eu_X:Gd_Y:Tb_Z-PCM-22Chart showing eight-factor fingerprint signatures obtained upon exposure to a range of chemical solvents. Each sphere is colored with the RGB coordinates obtained from the CIE charts (see examples on the right); the size of each sphere is representative of the relative brightness (emission intensity).

A reference chart was derived for comparison of the eight-factor fingerprints for each solvent (Figure 4). Each unique fingerprint is shown as four CIE colored spheres in which the visible size of each sphere is directly proportional to the magnitude of its brightness ($I_{relative}$). Solvents in the chart are organized by decreasing dielectric constant (polarity). Even for chemically similar solvents, the eight-factor fingerprint is definitive. For example, the C_1–C_3*n*-alcohols are differentiated by a decrease in brightness with increasing alkyl chain length, as well as a shift toward redder emission. Common ketones (acetone and butanone) and aromatics (benzene, pyridine, and toluene) are distinctly identifiable. Selectivity is not limited to changes in molecular volume; the halogenated solvents CH_2Cl_2 and CH_3Cl also show distinct differences as a result of the different quenching abilities of C–H versus C–Cl bonds.

To demonstrate the potential applicability of our sensor materials in conventional paper-based disposable sensors, we prepared model dip-stick assemblies by simply depositing small amounts of the as-synthesized materials onto glass slides by using spray glue to adhere the crystallites. The materials were desolvated in air with a heat gun and then immersed in different solvents, which induced immediate color changes that were seen when viewed under a 354 nm lamp (Figure 5). The dip sticks were easily reactivated by further heating and could be used repeatedly to provide the same response (for relevant PXRD and emission spectra, see Figures S16 and S17, respectively).

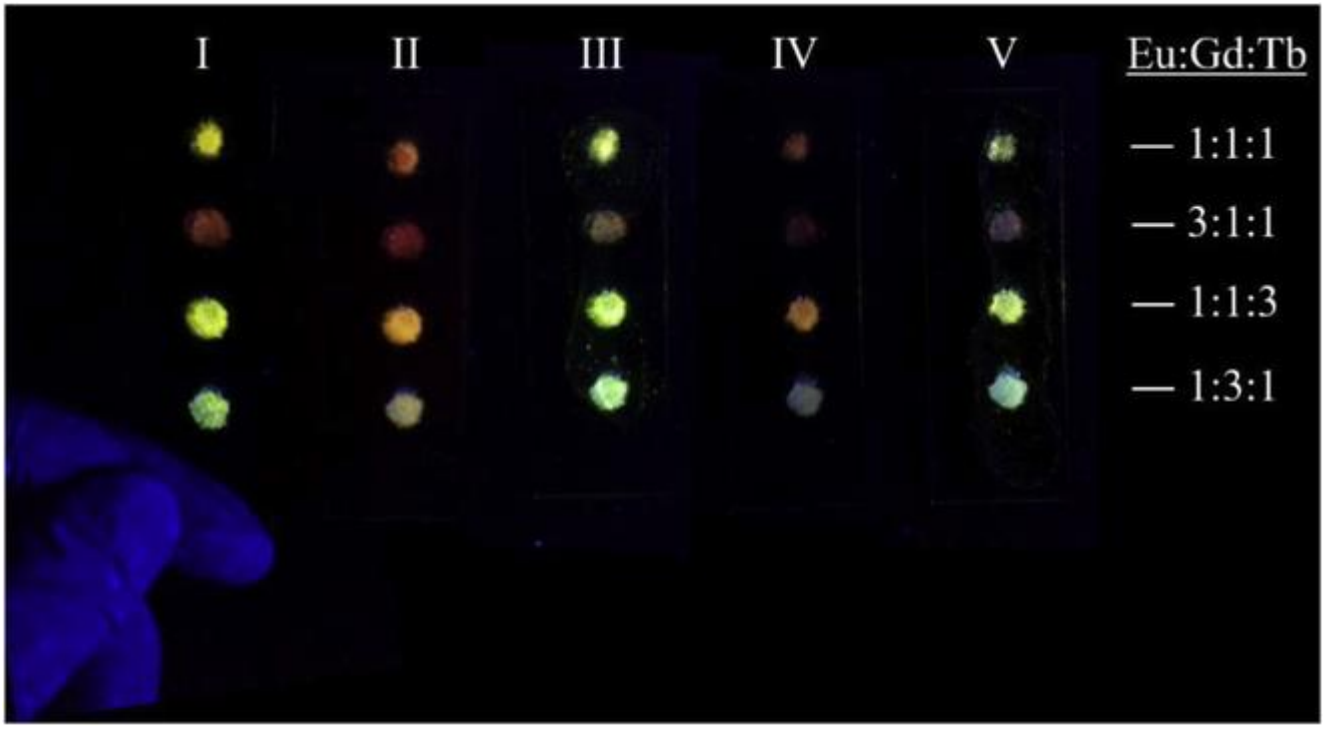

Figure 5 Broad Solvent Sensing Using Eu_X:Gd_Y:Tb_Z-PCM-22Model dip-stick detectors demonstrated for H_2O sensing: (I) as-synthesized, (II) desolvated in air with a heat gun, (III) after exposure to H_2O, (IV) re-activation using a heat gun, and (V) re-exposure to H_2O.

Experimental Procedures

A detailed explanation of all experimental methods and techniques used can be found in the Supplemental Information.

Synthesis of Ln-PCM-22

All Ln-PCM-22 materials were synthesized by the same method with appropriate proportions of lanthanide(III) nitrate hydrate precursors: in brief, tris(*p*-carboxylato)triphenylphosphine, $P(C_6H_4\text{-}4\text{-}CO_2H)_3$ (39 mg, 0.10 mmol) was dissolved in a DMF/dioxane/H_2O mixture (1:1:1, 4.0 cm^3; degassed by bubbling N_2 for at least 10 min before use). A second solution of the requisite $Ln(NO_3)_3 \cdot xH_2O$ salt(s) (0.20 mmol total) was prepared in the same solvent mixture (4.0 cm^3). The two solutions were then combined and agitated briefly before being heated in a (20 cm^3) scintillation vial by submersion to the solvent fill level in a pre-heated graphite thermal bath held at 80°C for 3–4 days. Crystalline products were recovered by decantation and washing with fresh solvent before being air dried. Full characterization and purification details for single-metal and mixed-metal Ln-PCM-22 materials are provided in the Supplemental Experimental Procedures.

Trace-Detection Studies

All dry crystalline materials were activated in small Schlenk flasks by heating at 100°C under vacuum via submersion for 18 hr in a silicone oil bath. Aliquots (2 mg) of the desolvated materials were used for each spectrophotometric measurement. Trace H_2O solvent mixtures were prepared by a series of serial dilutions from a known stock solution until the desired ppm concentrations were obtained. Further details, including the assembly of dip sticks, are given in the Supplemental Experimental Procedures.

Author Contributions

PCM-22 Synthesis and Characterization, S.G.D. and A.J.N.; Photophysical and Sensing Measurements, M.D.M.; Single Crystal XRD Data Analysis, A.S. and V.M.L.; Chemical Insight and Sensing Study Design, J.L.S.; Supervision of Photophysical Data Collection and Interpretation, B.J.H.; Project Design and Direction, S.M.H. All authors proofread, commented on, and approved the final version of this manuscript for submission.

Acknowledgments

We thank Prof. R.A. Jones for providing expert advice and for reviewing the manuscript and Dr. Nolan W. Waggoner for collecting BET data. This material is based on work supported by the National Science Foundation Division of Materials Research (DMR-1506994) and the Welch Foundation (F-1738 [S.M.H.] and chair funds [J.L.S.]).

Accession Numbers

The accession number for the data reported in this article is CCDC: 1518000.

Supplemental Information

Supplemental Information includes Supplemental Experimental Procedures, 17 figures, and 2 tables and can be found with this article online at http://dx.doi.org/10.1016/j.chempr.2017.02.010.

References and Notes

1. A.C. Grimsdale, K.L. Chan, R.E. Martin, P.G. Jokisz and A.B. Holmes, Synthesis of light-emitting conjugated polymers for applications in electroluminescent devices, *Chem. Rev.* **109**, 2009, 897–1091.

2. M.R. Kesama, S.R. Dugasani, S. Yoo, P. Chopade, B. Gnapareddy and S.H.Park, Morphological and optoelectronic characteristics of double and triple lanthanide ion-doped DNA thin films, *ACS Appl. Mater. Inter.* **8**, 2016, 14109–14117.

3. K. Binnemans, Lanthanide-based luminescent hybrid materials, *Chem. Rev.* **109**, 2009, 4283–4374.

4. S.V. Eliseeva and J.-C.G. Bünzli, Lanthanide luminescence for functional materials and bio-sciences, *Chem. Soc. Rev.* **39**, 2010, 189–227.

5. L.D. Carlos, R.A.S. Ferreira, V.D.Z. Bermudez and S.J.L. Ribeiro, Lanthanide-containing light-emitting organic-inorganic hybrids: a bet on the future, *Adv. Mater.* **21**, 2009, 509–534.

6. T. Gunnlaugsson and J.P. Leonard, Responsive lanthanide luminescent cyclen complexes: from switching/sensing to supramolecular architectures, *Chem. Commun.* 2005, 3114–3131.

7. S.E. Plush and T. Gunnlaugsson, Solution studies of trimetallic lanthanide luminescent anion sensors: towards ratiometric sensing using an internal reference channel, *Dalton Trans.* 2008, 3801–3804.

8. S.E. Plush and T. Gunnlaugsson, Luminescent sensing of dicarboxylates in water by a bismacrocyclic dinuclear Eu(III) conjugate, *Org. Lett.* **9**, 2007, 1919–1922.

9. N.W. Waggoner, A.M. Bohnsack and S.M. Humphrey, Metal-organic frameworks as chemical sensors, In: J.G. Hardy and F.H. Schecher, (Eds.), *Functional Metallosupramolecular Materials,* 2015, RSC Publishing, 192–235.

10. G. Tobin, S. Comby, N. Zhu, R. Clérac, T. Gunnlaugsson and W. Schmitt, Towards multifunctional lanthanide-based metal-organic frameworks, *Chem. Commun.* **51**, 2015, 13313–13316.

11. J.-M. Zhou, W. Shi, N. Xu and P. Cheng, Highly selective luminescent sensing of fluoride and organic small-molecule pollutants based on novel lanthanide metal–organic frameworks, *Inorg. Chem.* **52**, 2013, 8082–8090.

12. S.-N. Zhao, X.-Z. Song, M. Zhu, X. Meng, L.-L. Wu, S.-Y. Song, C. Wang and H.-J. Zhang, Highly thermostable lanthanide metal–organic frameworks exhibiting unique selectivity for nitro explosives, *RSC Adv.* **5**, 2015, 93–98.

13. B.V. Harbuzaru, A. Corma, F. Rey, J.L. Jordá, D. Ananias, L.D. Carlos and J.Rocha, A miniaturized linear pH sensor based on a highly photoluminescent self-assembled europium(III) metal-organic framework, *Angew. Chem. Int. Ed.* **48**, 2009, 6476–6479.

14. X. Liu, S. Akerboom, M. de Jong, S. Tanase, A. Meijerink and E. Bouman, Mixed-lanthanoid metal–organic framework for ratiometric cryogenic temperature sensing, *Inorg. Chem.* **54**, 2015, 11323–11329.

15. J.-N. Hao and B. Yan, Recyclable lanthanide-functionalized MOF hybrids to determine hippuric acid in urine as a biological index of toluene exposure, *Chem. Commun.* **51**, 2015, 14509–14512.

16. N.W. Waggoner, B. Saccoccia, I.A. Ibarra, V.M. Lynch, P.T. Wood and S.M.Humphrey, Magn etism of linear $[Ln_3]^{9+}$ oxo-bridged clusters (Ln = Pr, Nd) supported inside a $[R_3PR']$ phosphonium coordination material, *Inorg. Chem.* **53**, 2014, 12674–12676.

17. I.A. Ibarra, T.W. Hesterberg, B.J. Holliday, V.M. Lynch and S.M. Humphrey, Gas sorption and luminescence properties of a terbium(iii)-phosphine oxide coordination material with two-dimensional pore topology, *Dalton Trans.* **41**, 2012, 8003–8009.

18. I.A. Ibarra, T.W. Hesterberg, J.S. Chang, J.W. Yoon, B.J. Holliday and S.M.Humphrey, Molecu lar sensing and discrimination by a luminescent terbium–phosphine oxide coordination material, *Chem. Commun.* **49**, 2013, 7156–7158.

19. J. Mitchell, Karl Fischer reagent titration, *Anal. Chem.* **23**, 1951, 1069–1075.

20. Slizard, L. 1958. Heavy water moderated neutronic reactor. US Patent US2832733A, filed April 23, 1946, and published April 29, 1958.

21. K.B. Wiberg, The deuterium isotope effect, *Chem. Rev.* **55**, 1955, 713–743.

22. G. Meijer, J.J.T. Meulen, P. Andresen and A. Bath, Sensitive quantum state selective detection of H_2O and D_2O by (2+1)-resonance enhanced multiphoton ionization, *J. Chem. Phys.* **85**, 1986, 6914–6922.

23. Creasy, W.R., McGarvey, D.J., Rice, J.S., O'Connor, R., Durst, H.D. (2003). Study of detection limits and quantitation accuracy using 300 MHz NMR. ADA482893. www.dtic.mil/cgi-bin/GetTRDoc?AD=ADA482893.

24. D.K. Armani, T.J. Kippenberg, S.M. Spillane and K.J. Vahala, Ultra-high-Q toroid microcavity on a chip, *Nature* **421**, 2003, 925–928.

25. A.M. Armani and K.J. Vahala, Heavy water detection using ultra-high-Q microcavities, *Opt. Lett.* **31**, 2006, 1896–1898.

26. P. Atkins, T. Overton, J. Rourke, M. Weller and F. Armstrong, Shriver & Atkins' Inorganic Chemistry, 2010, Oxford University Press.

27. A.P. Côté, H.M. El-Kaderi, H. Furukawa, J.R. Hunt and O.M. Yaghi, Reticular synthesis of microporous and mesoporous 2D covalent organic frameworks, *J. Am. Chem. Soc.* **129**, 2007, 12914–12915.

28. M. Zhang, G. Feng, Z. Song, Y.P. Zhou, H.Y. Chao, D. Yuan, T.T. Tan, Z. Guo, Z. Hu, B.Z. Ta ng, et al., Two-dimensional metal–organic framework with wide channels and responsive

turn-on fluorescence for the chemical sensing of volatile organic compounds, *J. Am. Chem. Soc.* **136**, 2014, 7241–7244.

29. S.M. Humphrey, P.K. Allan, S.E. Oungoulian, M.S. Ironside and E.R. Wise, Metal–organophosphine and metal–organophosphonium frameworks with layered honeycomb-like structures, *Dalton Trans.* 2009, 2298–2305.

30. J. Feng and H. Zhang, Hybrid materials based on lanthanide organic complexes: a review, *Chem. Soc. Rev.* **42**, 2013, 387–410.

31. J.-C.G. Bünzli and S.V. Eliseeva, Basics of lanthanide photophysics, In: P.Hänninen and H. Härmä, (Eds.), *Lanthanide Luminescence, Springer Series on Fluorescence* **vol. 7**, 2010, Springer, 1–45.

32. T. Fiedler, M. Hilder, P.C. Junk, U.H. Kynast, M.M. Lezhnina and M. Warzala, Synthesis, structural and spectroscopic studies on the lanthanoid p-aminobenzoates and derived optically functional polyurethane composites, *Eur. J. Inorg. Chem.* **2007**, 2007, 291–301.

33. J.-C.G. Bünzli and C. Piguet, Taking advantage of luminescent lanthanide ions, *Chem. Soc. Rev.* **34**, 2005, 1048–1077.

34. Z.-J. Lin, B. Xu, T.-F. Liu, M.-N. Cao, J. Lü and R. Cao, A series of lanthanide metal-organic frameworks based on biphenyl-3,4′,5-tricarboxylate: syntheses, structures, luminescence and magnetic properties, *Eur. J. Inorg. Chem.* **2010**, 2010, 3842–3849.

35. D.T.D. Lill, A.D. Bettencourt-Dias and C.L. Cahill, Exploring lanthanide luminescence in metal-organic frameworks: synthesis, structure, and guest-sensitized luminescence of a mixed europium/terbium-adipate framework and a terbium-adipate framework, *Inorg. Chem.* **46**, 2007, 3960–3965.

36. H. Sato, W. Kosaka, R. Matsuda, A. Hori, Y. Hijikata, R.V. Belosludov, S.Sakaki, M. Takata an d S. Kitagawa, Self-accelerating CO sorption in a soft nanoporous crystal, *Science* **343**, 2013, 167–170.

37. Y. Cui, H. Xu, Y. Yue, Z. Guo, J. Yu, Z. Chen, J. Gao, Y. Yang, G. Qian and B.Chen, A luminescent mixed-lanthanide metal–organic framework thermometer, *J. Am. Chem. Soc.* **134**, 2012, 3979–3982.

38. I. Laulicht and S. Meirman, Direct evidence for excitation transfer from the $^5D_4$ manifold of Tb_3 to the $^5D_1$ manifold of Eu_3 in $Tb_{0.66}Eu_{0.33}P_5O_{14}$, *J. Lumin.* **34**, 1986, 287–293.